Surface Radiation Effects on Flame Spread Over Thermally Thick Fuels in an Opposing Flow

J. West

S. Bhattacharjee

Department of Mechanical Engineering,
San Diego State University,
San Diego, CA 92182

R. A. Altenkirch

Department of Mechanical Engineering, and
NSF Engineering Research Center for
Computational Field Simulation,
Mississippi State University,
Mississippi State, MS 39762

A computational model of flame spread over a thermally thick solid fuel in an opposing-flow environment is presented. Unlike thermally thin fuels, for which the effect of fuel surface radiation is negligiible for high levels of opposing flow, fuel surface radiation is important for thermally thick fuels for all flow levels. This result is shown to derive from the fact that the ratio of the rate of heat transfer by re-radiation from the surface to that by conduction from the gas to the solid is proportional to the length over which heat can be conducted forward of the flame to sustain spreading. For thin fuels, this length decreases with increasing flow velocity such that while radiation is important at low flow velocities it is not at the higher velocities. For thick fuels at low flow velocities, the conduction length is determined by gas-phase processes and decreases with increasing flow velocity. But at higher flow velocities, the conduction length is determined by solid-phase processes and is rather independent of the gas-phase flow. The result is that over a wide range of flow velocities, the conduction length of importance does not change substantially as it switches from one phase to another so that the ratio of radiation to conduction is of unit order throughout that wide range of flow.

Introduction

The importance of understanding the governing mechanisms of flame spread is well established. Much experimental and analytical work has been carried out to determine flame spread mechanisms in normal and elevated convection levels for both thermally thin and thick fuels (e.g., de Ris, 1969; Frey and T'ien, 1979; Altenkirch et al., 1980; Fernandez-Pello et al., 1981; Mao et al., 1984; Olson et al., 1989; Altenkirch et al., 1983, Altenkirch and Bhattacharjee, 1990; Bhattacharjee and Altenkirch, 1990, 1991; Bhattacharjee et al., 1990, 1991). However, little has been done to investigate the behavior of thermally thick flame spread between, and including, the quiescent environment limit and moderate forced opposed convection where the effects of buoyancy are comparable to those of the forced flow.

de Ris (1969), in his analytical solution for the flame spread rate, $\hat{V}_f$, found the flame spread rate to be independent of the opposing velocity, $\hat{V}_g$, for thermally thin fuels and proportional to $\hat{V}_g$ for thermally thick fuels. The analytical solution was produced under the assumption of infinite-rate chemical kinetics and thus applies only to low levels of opposing convection and/or high levels of oxygen in the flow. The velocity field was prescribed as an Oseen flow, and assumptions were made regarding the fluid and fuel properties to allow a solution to be obtained.

Fernandez-Pello et al. (1981), in their experimental study, investigated the effect of opposing convection level and ambient oxygen concentration on the flame spread rate over thermally thick sheets of polymethylmethacrylate (PMMA). Their study confirmed the behavior of the flame spread rate as a function of opposing convection and ambient oxygen concentration as predicted by de Ris for low forced convective levels.

Previous numerical models for thermally thick fuels (Di Blasi et al., 1987, 1988) employ a constant pressure and a prescribed flow field and neglect any radiative process. Additionally results for various ambient oxgyen concentrations for a fixed heat of combustion (Di Blasi et al., 1988) resulted in flame temperatures well in excess of physically realistic and/or known levels.

Studies that include the effects of either gas and/or fuel surface radiation on thermally thin fuels were conducted by Altenkirch and Bhattacharjee (1990) and Bhattacharjee and Altenkirch (1990, 1991). The former effort produced scaling arguments about the relative importance of heat conduction to radiative heat transfer over different flame spread regimes, while the latter studies were ones in which a numerical model, including both gas-phase and fuel surface radiation, was used to obtain predictions of the near-quiescent flame spread rate over a thermally thin fuel.

Here a model, similar to previously presented numerical models (Bhattacharjee et al., 1990; Bhattacharjee and Altenkirch, 1990, 1991), that couples the gas-phase flow field to prediction of the thermally thick flame spread rate and additionally considers the effects of fuel surface radiative loss is presented. This model will be used to investigate the importance of radiative effects for flame spread over thick fuels, particularly at the low flow velocities where radiative effects affect flame spread over thin fuels. Gas-phase radiation, although potentially important at near-quiescent conditions such as those that can be obtained in the microgravity environment of spacecraft, is neglected in favor of considering the major radiative effect as a heat loss from the fuel surface to the ambient environment (Bhattacharjee and Altenkirch, 1990; Bhattacharjee et al., 1991).

Problem Formulation

The flame spread model consists of the elliptic, partial differential equations describing conservation of mass, energy, momentum, and species in the gas phase and the elliptic partial differential equation describing conservation of energy in the solid phase. The gas-phase equations are written in steady-state form for a single-step, Arrhenius reaction and solved in flame-fixed coordinates such that the flame sees an opposing, forced flow of velocity equal to the flame spread rate plus any forced opposing velocity, if present. Because the gas-phase

Contributed by the Heat Transfer Division and presented at the National Heat Transfer Conference, San Diego, California, August 9–12, 1992. Manuscript received by the Heat Transfer Division December 1992; revision received July 1993. Keywords: Fire/Flames, Microgravity Heat Transfer, Radiation Interactions. Associate Technical Editor: W. L. Grosshandler.

Table 1 Equation coefficients for the gas phase

Equation	ø	$\Gamma_ø$	$S_ø$
Continuity	1	0	0
x-momentum	$u=\hat{u}/\hat{V}_r$	μ/Pr	$-\partial P/\partial x$
y-momentum	$v=\hat{v}/\hat{V}_r$	μ/Pr	$-\partial P/\partial y$
Fuel	m_f	μ	$-Da_g\rho^2 m_{ox} m_f\, e^{-Eg/T}$
Oxygen	m_{ox}	μ	$-sDa_g\rho^2 m_{ox} m_f\, e^{-Eg/T}$
Energy	$T=\hat{T}/\hat{T}_\infty$	μ	$\Delta H_c Da_g\rho^2 m_{ox} m_f\, e^{-Eg/T}$

formulation is similar to that given elsewhere (Bhattacharjee et al., 1990), only a brief description is presented.

A velocity characteristic of the gas, $\hat{V}_r$, which is the sum of the forced convective velocity, $\hat{V}_g$, and the flame spread rate, $\hat{V}_f$, is used as the unit in which velocities are measured. This velocity is used to develop the thermal length in the gas, $\hat{L}_r = \hat{\alpha}_r/\hat{V}_r$, which is the unit in which all lengths are measured. The gas-phase thermal diffusivity is evaluated at a reference temperature, $\hat{T}_r$, which is the average of the adiabatic, stoichiometric flame temperature neglecting dissociation and the ambient temperature.

The conservation equations in the gas may be written in the same common form as in Eq. (1) where the various ϕ's, Γ_ϕ's and S_ϕ's are given in Table 1:

$$\frac{\partial(\rho u\phi)}{\partial x}+\frac{\partial(\rho v\phi)}{\partial y}=\frac{\partial}{\partial x}\left\{\Gamma_\phi\frac{\partial(\phi)}{\partial x}\right\}+\frac{\partial}{\partial y}\left\{\Gamma_\phi\frac{\partial(\phi)}{\partial y}\right\}+S_\phi \quad (1)$$

Contributions to the momentum sources due to the compressible nature of the flow were found to be negligible for this type of flow (Bhattacharjee et al., 1990), and so they are neglected.

To solve for the seven unknowns in the gas phase, i.e., u, v, P, T, ρ, m_f, and m_{ox}, the six conservation equations along with the equation of state, $\rho T = \hat{\rho}_\infty/\hat{\rho}_r$, and a square root dependence of viscosity and thermal conductivity on temperature are used. The computational domain for the gas-phase equations is a two-dimensional x-y coordinate system with origin located on the fuel surface at the rear of the computational domain. The x direction is along the fuel surface with positive x upstream and y direction is normal to the fuel surface with positive y into the gas. Boundary conditions suitable for the modeling of forced convective flows are the following:

Upstream at $x=x_{\max}$,

$$u=(v_f+v_g),\ v=0,\ m_f=0,\ m_{ox}=m_{ox,\infty},\ T=1,\ P=0$$

Downstream at $x=0$,

$$\text{all}\ \frac{\partial\phi}{\partial x}=0$$

At $y=y_{\max}$,

$$u=-(v_f+v_g),\ \frac{\partial v}{\partial y}=0,\ m_f=0,\ m_{ox}=m_{ox,\infty},\ T=1,\ P=0$$

at $y=0$,

$$u=-v_f,\ v=v_w,\ T=T_s \quad (2)$$

The quantities v_f, v_w, and T_s are obtained from the solution to the solid-phase problem, while m_f and m_{ox} at $y=0$ are obtained from an interfacial species balance, Eqs. (3) and (4), respectively. The meanings of ϕ and Γ_ϕ are given in Table 1:

$$\left(\rho v_w\phi+\Gamma_\phi\frac{\partial(\phi)}{\partial y}\right)\Bigg|_{y=0}=\rho v_w \quad (3)$$

$$\left(\rho v_w\phi+\Gamma_\phi\frac{\partial(\phi)}{\partial y}\right)_{y=0}=0 \quad (4)$$

The gas-phase length and velocity scales were used to write the solid-phase energy equation in dimensionless form:

$$-v_f\frac{\partial T_s}{\partial x}=\frac{\partial}{\partial x}\left\{\alpha_s\frac{\partial T_s}{\partial x}\right\}+\frac{\partial}{\partial y}\left\{\alpha_s\frac{\partial T_s}{\partial y}\right\} \quad (5)$$

The boundary conditions for this equation, including a surface

Nomenclature

$\hat{A}_s$ = pre-exponential factor for solid pyrolysis = 2.82×10^9 s^{-1}

$\hat{B}_g$ = frequency factor for the gas-phase reaction = 5.982×10^9 $m^3/kg\cdot s$

$\hat{C}_g$ = specific heat at constant pressure for the gas, kJ/kg·K (see Table 2)

$\hat{C}_s$ = specific heat of the solid fuel = 1.465 kJ/kg·K

Da_g = Damkohler number in the gas phase = $\hat{\rho}_r\hat{B}_g\hat{L}_r/\hat{V}_R$

E_g = dimensionless activation energy in the gas phase = $\hat{E}_g\overline{R}/\hat{T}_\infty$

$\hat{E}_g$ = gas-phase activation energy = 1.424×10^5kJ/kmol

$\hat{E}_s$ = solid-phase activation energy = 1.298×10^5kJ/kmol

$\hat{L}_r$ = reference thermal length = $\hat{\alpha}_r/(\hat{V}_g+\hat{V}_f)$, m

$\hat{L}_g$ = thermal length in the gas phase = $\hat{\alpha}_g/\hat{V}_g$ for small $\hat{V}_f$, in both x and y directions, m

$\hat{L}_{sx}$ = thermal length in the solid phase in the x direction = $\hat{\alpha}_s/\hat{V}_f$, m

L_v = dimensionless effective latent heat of evaporation = $\hat{L}_v/\hat{C}_s\hat{T}_\infty$

$\hat{L}_v$ = effective latent heat of evaporation = $\hat{L}_v^o+(\hat{C}_g-\hat{C}_s)(\hat{T}_s-\hat{T}_\infty$, kJ/kg

$\hat{L}_v^o$ = latent heat of evaporation for PMMA at 298 K, = 941 kJ/kg

$\dot{m}''$ = dimensionless mass = $\dot{\hat{m}}''/\hat{\rho}_s\hat{V}_r$

$\dot{\hat{m}}''$ = mass flux from fuel to the gas phase, $kg/m^2\cdot s$

$\hat{M}_f$ = molecular weight of PMMA = 100 kg/kmol

$\hat{M}_{ox}$ = molecular weight of oxygen = 32 kg/kmol

m_f = mass fraction of fuel in the gas phase

m_{ox} = mass fraction of oxygen in the gas phase

$m_{ox,\infty}$ = mass fraction of oxygen for ambient conditions

P = dimensionless pressure = $(\hat{P}-\hat{P}_\infty)/(\hat{\rho}_r\hat{V}2_r)$

$\hat{P}$ = pressure, N/m^2

Pr_r = reference Prandtl number for the gas = $\hat{\mu}_r\hat{C}_g/\hat{\lambda}_r$

$\hat{Q}_{gsc}$ = gas-phase to solid-phase heat conduction = $\hat{\lambda}_g(\hat{T}_f-\hat{T}_v)_g\hat{L}_g w/\hat{L}_g$, W

$\dot{\hat{q}}_{net}$ = net heat flux incoming to the fuel surface, W/m^2

$\dot{q}_{net}$ = dimensionless net heat flux to the fuel surface = $\dot{\hat{q}}_{net}/(\hat{\rho}_s\hat{C}_s\hat{T}_\infty\hat{V}_r)$

$\hat{Q}_{rad}$ = solid-phase surface radiative heat loss = $\hat{\sigma}\epsilon(\hat{T}_f^4-\hat{T}_v^4)\hat{L}_{sx}w$, W

$\overline{R}$ = universal gas constant = 8.314 kJ/kmol·K

S_c = conduction/convection parameter = $\hat{\lambda}_r/(\hat{\rho}_s\hat{L}_r\hat{V}_r\hat{C}_s)$

S_R = radiation/conduction parameter = $\epsilon\hat{\sigma}\hat{T}_\infty^3/(\hat{\rho}_s\hat{C}_s\hat{V}_r)$

S_ϕ = source term for property ϕ

s = stoichiometric ratio = $\hat{M}_{ox}\nu_{ox}/\hat{M}_f\nu f$ = 1.92

T = dimensionless gas temperature $\hat{T}/\hat{T}_\infty$

$\hat{T}$ = gas temperature, K

$\hat{T}_f$ = flame temperature used in scaling, K

$\hat{T}_r$ = reference temperature for the gas, K (see Table 2)

T_s = dimensionless solid temperature = $\hat{T}_s/\hat{T}_\infty$

$\hat{T}_s$ = solid temperature, K

$\hat{T}_v$ = pyrolysis temperature used in scaling = 700 K

$\hat{T}_\infty$ = ambient temperature = 298 K

u = dimensionless x velocity = $\hat{u}/\hat{V}_r$

radiative loss term, which is the only radiative effect considered in this model, are:

$$\text{at } x = x_{\max}: \quad T_s = 1$$

$$\text{at } x = 0: \quad \frac{\partial T_s}{\partial x} = 0$$

$$\text{at } y = y_{\min} < 0: \quad \frac{\partial T_s}{\partial y} = 0$$

$$\text{at } y = 0: \quad \dot{q}''_{\text{net}} = S_c \mu \left.\frac{\partial T}{\partial y}\right|_{y=0} - S_R\,(T_{s-1}^4) - \dot{m}'' L_v \quad (6)$$

The solid thickness and density are assumed to be constant, with the mass of the fuel evaporated considered to be negligible in comparison to the total amount of fuel available for pyrolysis. Clearly this assumption could lead to violation of mass conservation in the model. For the computations presented here the amount of fuel pyrolyzed was never more than the amount of fuel entering the computational domain. However, when the amount of fuel evaporated is on the order of the amount of fuel available, the neglect of the mass conservation equation in the solid may cause appreciable error in the energy equation as well. This situation occurred only when small fuel thicknesses were modeled, i.e., when the fuel half-thickness, $\hat{\tau}$, was equal to or less than about 0.05 cm. The neglect of solid-phase mass conservation also precluded taking into account any effect of fuel surface regression, which may become important at high opposing velocities (Altenkirch et al., 1982).

The expression for the pyrolysis mass flux of the solid fuel that is used in Eq. (6) was developed from a solution to the one-dimensional energy equation obtained by Lengelle (1970) in which the regression rate for the fuel surface was obtained from an asymptotic expansion for the solid temperature field for large activation energy of pyrolysis. The numerical values in Eq. (7) arise from an assumed residual density, $\hat{\rho}_s/\hat{\rho}_{s,\infty} = 0.01$, which allows the solution to be obtained:

$$\hat{\dot{m}}'' = \left\{\frac{\hat{\rho}\hat{T}_s^2 \hat{A}_s \hat{\lambda}_s \bar{R}}{\hat{E}_s[3.615\hat{L}_v^o + 4.605\hat{C}_s(\hat{T}_s - \hat{T}_\infty)]}\right\}^{1/2} \exp\left(\frac{-E_s}{2\bar{R}\hat{T}_s}\right) \quad (7)$$

In order to determine the two unknowns T_s and $\hat{V}_f$, another condition other than the solid surface energy balance and the boundary conditions on T_s is needed. This condition was provided by determining the flame spread rate $\hat{V}_f$ such that the flame leading edge is fixed at a certain x location near the front of the computational domain. This entailed increasing $\hat{V}_f$ if the flame started to progress ahead of this point to retard the progression and decreasing $\hat{V}_f$ if the flame started to fall behind this point. The flame leading edge was identified by a solid surface temperature of 1.2 $\hat{T}_\infty$, the eigen temperature. This choice of the eigen temperature only fixes the location of the flame in the computational domain; by changing this value, the location of the flame within the computational domain is shifted slightly, leaving all other aspects of the solution unchanged.

The heat of combustion and specific heat were defined as functions of the ambient oxygen concentration in order to approximate the effects of gas-phase chemical dissociation. The method was identical to that of West et al. (1992) and consists of determining the equilibrium product distribution and flame temperature for adiabatic, stoichiometric combustion of the solid fuel and defining the heat of combustion and constant, gas-phase specific heat to be consistent with this calculation.

The combustion process is modeled using a one-step, second-order Arrhenius reaction. The gas-phase kinetic properties, i.e., pre-exponential factor and activation energy, were selected from a range of values that appear in the literature for PMMA that also resulted in computations that matched low-oxygen, high forced convection experimental results (Fernandez-Pello

Nomenclature (cont.)

$\hat{u}$ = x velocity, m/s
$\hat{V}_f$ = absolute value of flame spread rate, m/s
$\hat{V}_g$ = absolute value of opposing gas velocity, m/s
$\hat{V}_r$ = reference velocity (= $\hat{V}_f$ in a quiescent environment), m/s
$\hat{V}_w$ = velocity at the fuel surface normal to the surface, m/s
v = dimensionless y velocity = $\hat{v}/\hat{V}_r$
$\hat{v}$ = y velocity, m/s
V_f = dimensionless spread rate = $\hat{V}_f/\hat{V}_r$
V_g = dimensionless opposing gas velocity = $\hat{V}_g/\hat{V}_r$
v_w = dimensionless velocity at the fuel surface normal to the surface = $\hat{V}_w/\hat{V}_r$
$\hat{w}$ = width of fuel sample; model is independent of this value, m
x = dimensionless coordinate parallel to fuel surface = $\hat{x}/\hat{L}_r$
$\hat{x}$ = coordinate parellel to the fuel surface, m
$x_{\min}$ = minimum x in computational domain, $x = 0$
$x_{\max}$ = maximum x in computational domain, $x = 28$
y = dimensionless coordinate normal to the fuel surface = $\hat{y}/\hat{L}_r$
$\hat{y}$ = coordinate normal to the fuel surface, m
$y_{\max}$ = maximum y in the computational domain, $y = 28$
$\hat{\alpha}_r$ = reference thermal diffusivity of the gas, m^2/s
$\hat{\alpha}_s$ = thermal diffusivity of the solid, m^2
α_s = dimensionless thermal diffusivity of the solid = $\hat{\alpha}_s/\hat{\alpha}_r$
Γ_ϕ = dimensionless viscosity = $\mathrm{Pr}_r\mu$ or μ
ΔH_c = dimensionless heat of combustion = $\Delta\hat{H}_c/\hat{C}_g\hat{T}_\infty$
$\Delta\hat{H}_c$ = heat of combustion of PMMA, kJ/kg (see Table 2)
ϵ = emittance of the fuel surface
$\hat{\lambda}_r$ = thermal conductivity of the gas, W/m·K (see Table 2)
μ = dimensionless dynamic viscosity = $\hat{\mu}/\hat{\mu}_r$
$\hat{\mu}_r$ = reference dynamic viscosity, kg/m·s (see Table 2)
ν_f = stoichiometric coefficient for fuel
ν_{ox} = stoichiometric coefficient for oxygen
ρ = dimensionless gas density = $\hat{\rho}/\hat{\rho}_r$
$\hat{\rho}_r$ = reference density for the gas, kg/m^3 (see Table 2)
ρ_s = dimensionless solid density = $\hat{\rho}_s/\hat{\rho}_{s,\infty}$
$\hat{\rho}_\infty$ = ambient gas density, kg/m^3
σ = Stefan–Boltzmann constant = 5.67×10^{-8} W/m^2·K^4
$\hat{\tau}$ = half-thickness of the fuel sheet, m
ϕ = any dimensionless dependent variable = $\hat{\phi}/\hat{\phi}_r$

Subscripts

f = fuel
g = gas
ox = oxygen
R = radiation
r = reference state
rad = radiation
s = solid
∞ = ambient

Superscripts

$\hat{}$ = dimensional quantity
$''$ = per unit area
$'$ = per unit length

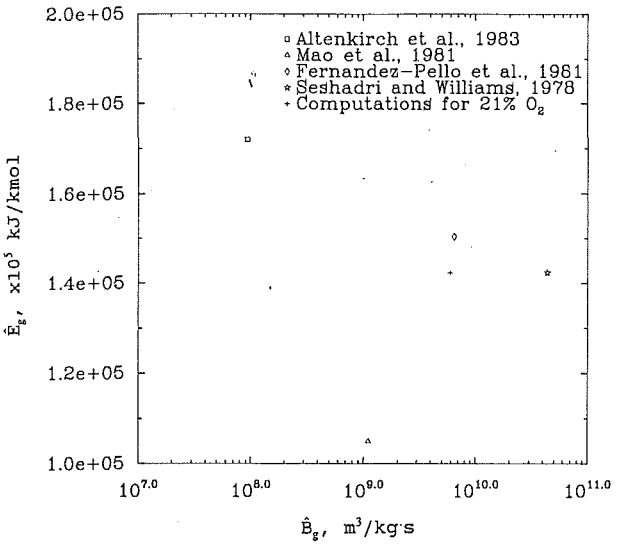

Fig. 1 Chemical kinetic properties used in modeling PMMA combustion. Also the property combination, indicated by the plus symbol, that reproduces the maximum experimental spread rate at 21 percent O_2 in N_2 and 1 atm pressure, neglecting radiation.

Table 2 Properties for the gas-phase calculations

Property	Pressure atm	Ambient O_2 21%	Ambient O_2 30%	Ambient O_2 50%
$\hat{T}_r$ (K)	any	1312	1565	1959
$\hat{\mu}_r$ (x10^5, kg/m·s)	any	4.812	5.567	6.629
$\hat{\lambda}_s$ (x10^2, W/m·K)	any	6.853	7.550	5.615
$\hat{C}_g$ (kJ/kg·K)	any	1.299	1.356	1.447
$\hat{\rho}_r$ (kg/m^3)	1.5	0.401	0.341	0.280
$\Delta\hat{H}_c$ (x10^{-3}, kJ/kg)	any	24.24	21.54	17.53

et al., 1981). The level of opposing velocity used to find the computational match to experiment was the one that produced the maximum experimental spread rate at 21 percent oxygen. This is illustrated in Fig. 1, a presentation of PMMA kinetic properties used by others along with a combination of kinetic properties that reproduces the maximum experimental spread rate at 21 percent oxygen by volume at 1 atm pressure when used in computations neglecting all radiative processes.

There are an infinite number of kinetic property combinations that reproduce the experimental results. Consequently, a combination that is both representative of values used by others for modeling PMMA combustion and which matches the activation energy from experimental results obtained by Seshadri and Williams (1979) was chosen. The values are $B_g = 5.92 \times 10^9$ m^3/kg·s and $\hat{E}_g = 1.424 \times 10^5$ kJ/kmol.

The gas-phase kinetic constants were chosen using data at 21 percent ambient oxygen concentration because no combination of constants could be found that allowed experimental spread rates to be matched at both 21 percent and the higher oxygen concentrations for the heats of combustion listed in Table 2. This difficulty can likely be traced to the fact that the spread rate for a thick fuel is sensitive to flame temperature, i.e., it depends approximately on the square of the difference between the flame and vaporization temperatures (de Ris, 1969). Accurate prediction of flame temperature is then needed over a range of oxygen concentrations in order to yield good agreement between measured and predicted spread rates over that range. While the adiabatic dissociation model used here to establish heats of combustion as a function of ambient oxygen concentration is more realistic than using a fixed heat of combustion, it does not take into account the fact that the extent of dissociation compared to the maximum for the adiabatic situation is variable because of radiative losses from the flame.

The environmental conditions for the base case are 50 percent O_2 in N_2 by mass at 1 atm pressure with an opposing velocity ranging from 1 to 80 cm/s and a fuel half-thickness of 5 cm. Unless otherwise stated, the results presented will neglect fuel surface radiative loss. Values for the gas-phase dynamic viscosity and thermal conductivity were taken from Touloukian (1970). Properties for PMMA were taken from Lengelle (1970) and are: $\hat{C}_s = 1.465$ kJ/kg·K, $\hat{L}_v^o = 941$ kJ/kg$_{\text{fuel}}$, $\hat{\rho}_s = 1190$ kg/m^3, $\hat{\lambda}_s = 0.209$ W/m·K, and $\hat{M}_f = 100$ kg/kmol.

The gas- and solid-phase equations are solved separately using a control volume algorithm (Patankar, 1980). The computational domain in the gas phase was 28 thermal lengths per side with a nonuniform 60×42 grid with the highest concentration of grid points near the leading edge of the flame. The computational domain in the solid phase was 28 gas-phase thermal lengths in the x direction with the required number of gas-phase length scales in the y direction to conform to the solid thickness being considered. The solid-phase grid size was 60×20 with the highest concentration of grid points near the fuel surface.

The computational domain was sized to insure that the flame was embedded in the boundary layer removed from the leading edge of the fuel sample where the boundary layer begins to grow. For flame spreading against a forced flow, the distance from the flame leading edge to the leading edge of the fuel plate determines the strength of the opposing flow in the boundary layer there. From a practical standpoint, the spread rate becomes relatively insensitive to this distance, although in principle it is always dependent on it. Computational experience shows that if the distance between the leading edge of the flame and the fuel bed is greater than about 8 $\hat{L}_r$ the spread rate is insensitive to this distance. As a result, for all computations presented here this distance is never less than 8 $\hat{L}_r$.

Results and Discussion

The results of the computations are shown in Figs. 2 and 3, in which the computed spread rates as a function of fuel half-thickness, $\hat{\tau}$, are shown for flows of $\hat{V}_g = 5$ cm/s and 15 cm/s, respectively. In both figures the flame spread rate for small $\hat{\tau}$ decreases with increasing fuel thickness and then reaches a thick limit where any additional thickness increase has no effect on the flame spread rate.

de Ris (1969), in his analytical solution for the flame spread rate over thermally thin fuels, found that the flame spread rate was inversely proportional to the fuel half-thickness, $\hat{\tau}$; for thick fuels, the flame spread rate is proportional to the opposing velocity, $\hat{V}_g$. Thus the predicted behavior of the computations and de Ris's analytical results agree in that in the thermally thin regime the flame spread rate is inversely proportional to the fuel thickness, while beyond a thick limit the flame spread rate is no longer dependent on the fuel thickness.

Comparison of the figures reveals that the value of the thick limit is influenced by the level of opposing flow. For a given fuel thickness, an increase in the opposing velocity causes the fuel to resemble more closely a thermally thick fuel. Likewise, reducing the level of opposing flow for a given fuel thickness causes the fuel to behave more like a thermally thin fuel.

The results of the computations for the flame spread rate as a function of forced opposing flow are shown in Fig. 4, where the flame spread rate, $\hat{V}_f$, is presented as a function of the opposing velocity, $\hat{V}_g$, with and without considering the effects of fuel surface radiation. The flame spread rate initially

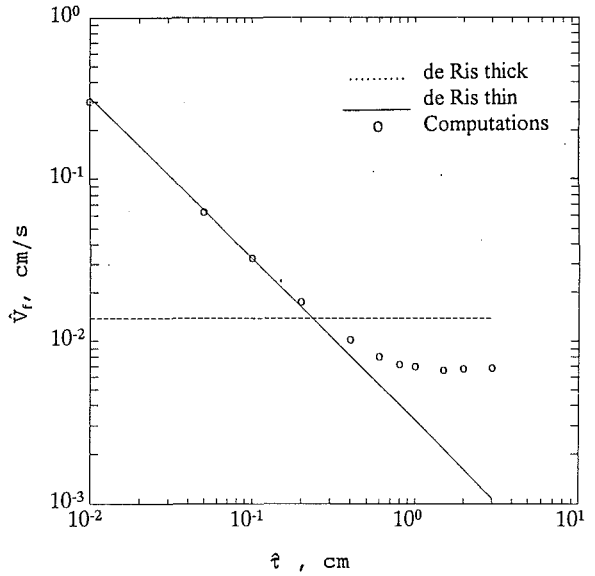

Fig. 2 Flame spread rate $\hat{V}_f$ as a function of fuel half-thickness, $\hat{\tau}$, for 50 percent O_2 in N_2 at 1 atm and opposing velocity, $\hat{V}_g$, of 5 cm/s neglecting fuel surface radiation

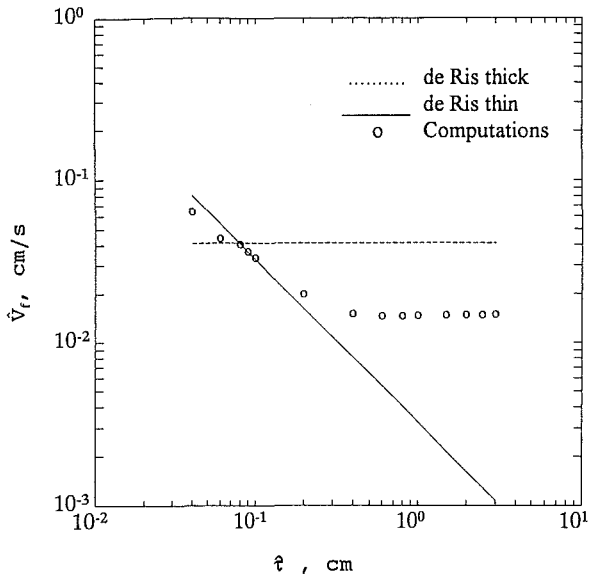

Fig. 3 Flame spread rate $\hat{V}_f$ as a function of fuel half-thickness, $\hat{\tau}$, for 50 percent O_2 in N_2 at 1 atm and opposing velocity, $\hat{V}_g$, of 15 cm/s neglecting fuel surface radiation

increases with increasing opposing flow velocity, reaches a maximum, and then decreases with increasing $\hat{V}_g$.

The initial increase of $\hat{V}_f$ is in the agreement with the de Ris result for thermally thick fuels, i.e., the flame spread rate is proportional to the opposing flow velocity. That the spread rate decreases after a limiting value of opposing flow is reached is due to the computational model's inclusion of finite-rate, gas-phase kinetics.

Figure 4 also shows that the effect of fuel surface radiation on the thermally thick flame spread rate is a net decrease in the spread rate. This net decrease does not go down with increasing opposing flow velocity as is predicted for thermally thin fuels (Altenkirch and Bhattacharjee, 1990; Bhattacharjee and Altenkirch, 1990; West et al., 1992).

Understanding of this difference may be obtained from scaling arguments similar to those of Alterkirch and Bhattacharjee (1990). There the relative importance between fuel surface radiative heat loss and gas-to-solid heat conduction for thin fuels was expressed as in Eq. (8), a ratio of heat loss from fuel

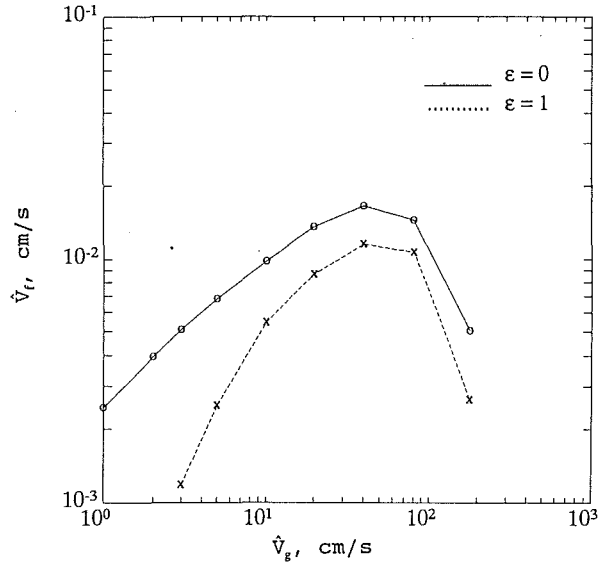

Fig. 4 Flame spread rate $\hat{V}_f$ as a function of opposing velocity, $\hat{V}_g$, for 50 percent O_2 in N_2 at 1 atm, fuel half-thickness, $\hat{\tau}$, of 5 cm with and without the effect of fuel surface radiation

surface radiation to the heat conducted from the flame to the fuel.

$$R_s = \frac{\hat{Q}_{\text{rad}}}{\hat{Q}_{gsc}} = \frac{\hat{\sigma}\epsilon(\hat{T}_v^4 - \hat{T}_\infty^4)\hat{L}_r}{\hat{\lambda}_g(\hat{T}_f - \hat{T}_v)} \tag{8}$$

For thermally thin fuels the only length scale of interest is the gas-phase length scale, $\hat{L}_g = \hat{\alpha}_g/\hat{V}_g$, therefore, $\hat{L}_r = \hat{L}_g$. Inserting this length into the above expression reveals that as the level of opposing velocity increases and $\hat{V}_f \ll \hat{V}_g$, the relative importance of fuel surface radiation decreases.

For fuels that are not thermally thin, conduction through the solid is an additional mechanism of heat transfer into the virgin fuel besides $\hat{Q}_{gsc}$. Nevertheless, the $\hat{Q}_{gsc}$ still plays a dominant role (Ito and Kashiwagi, 1986). The radiation number R_s, derived for thin fuels, should express the relative importance of surface radiation for non-thin fuels too. The only problem is to determine what is an appropriate $\hat{L}_r$ for the non-thin fuel.

For thermally thick fuels and low levels of opposing velocity, $\hat{V}_f$ is of the same order as $\hat{V}_g$ and $\hat{L}_g > \hat{L}_{sx}$ due to the density differences between the gas and solid fuel. Under these conditions the gas-phase scale is impressed upon the solid, and the problem scales with the gas phase as in the thermally thin case, $\hat{L}_r = \hat{L}_g$. Therefore, it is expected that R_s would be large enough that fuel surface radiation loss would result in an appreciable spread rate decrease.

For high levels of opposing velocity where $\hat{V}_f \ll \hat{V}_g$ and thus $\hat{L}_g < \hat{L}_{sx}$ (Altenkirch et al., 1983), the solid-phase length is dominant. This is also evident from Figs. 5 and 6, which compare the gas- and solid-phase temperature contours in the region of the flame anchor for base conditions, neglecting fuel surface radiation. The two situations shown correspond to opposing flow velocities, $\hat{V}_g$, of 5 and 80 cm/s, respectively. The flame anchor is identified as the location of maximum heat flux from the gas phase to the solid phase, $Q_{gsc,\max}$, and corresponds to $x = 0$ in the figure. In the case of Fig. 5 the greatest extent of heating in the front of the flame is accomplished in the gas phase while in Fig. 6 the greatest extent of heating ahead of the flame occurs in the solid phase.

Thus the transition of the scaling of the problem from the gas scale for small opposing velocity to the solid scale at large opposing velocity results in R_s being largely independent of opposing velocity. This nearly constant scaling for the thermally thick flame spread problem results in fuel surface ra-

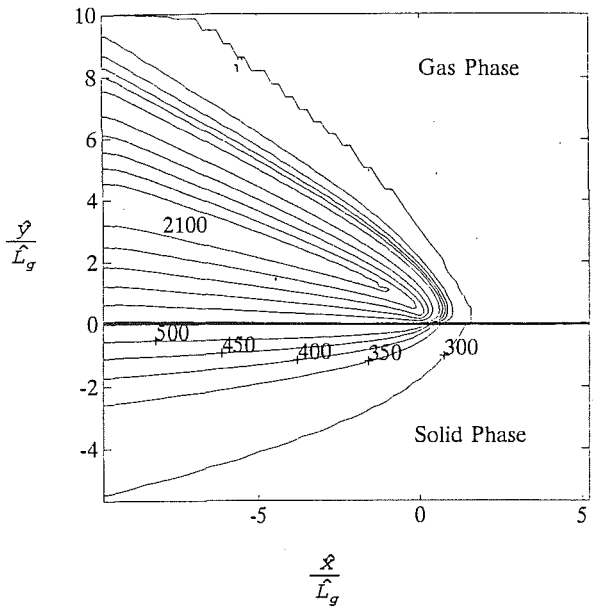

Fig. 5 Temperature contours, in K, for gas and solid phase showing greatest forward heat penetration occurring in the gas phase for an opposing flow velocity, $\hat{V}_g$, of 5 cm/s. Computation is for 50 percent O_2 in N_2 at 1 atm pressure and fuel half-thickness, $\hat{\tau}$, of 5 cm.

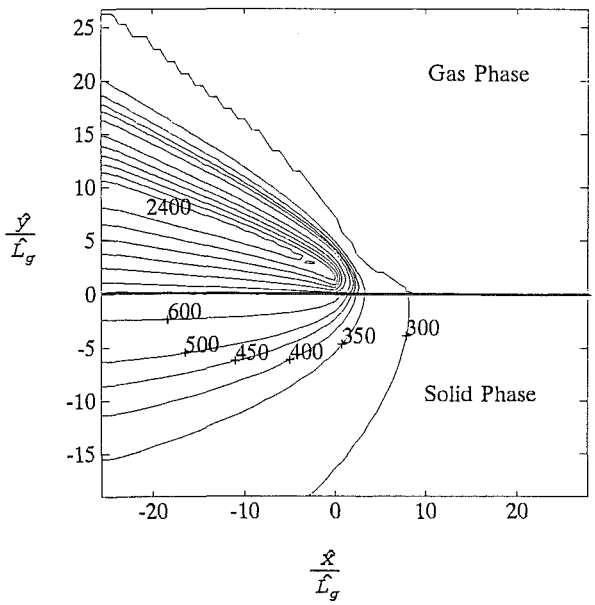

Fig. 6 Temperature contours, in K, for gas and solid phases showing greatest forward heat penetration occurring in the solid phase for an opposing flow velocity, $\hat{V}_g$, of 80 cm/s. Computation is for 50 percent O_2 in N_2 at 1 atm pressure and fuel half-thickness, $\hat{\tau}$, of 5 cm.

diation being important regardless of the level of opposing velocity.

Conclusions

In contrast to flame spread over thermally thin fuels, the effect of fuel surface radiation on the flame spread rate over thermally thick fuels is important regardless of level of opposing velocity. The effect of fuel surface radiation on the spread rate over thermally thin fuels has been found earlier to decrease with increasing opposing velocity. This difference can be explained by arguments that show that the x-direction length scale of the thermally thick problem is not markedly affected by the level of opposing velocity while the x-direction length scale of the thermally thin problem decreases with increasing opposing velocity.

Acknowledgments

Support for this work from NASA through Contracts No. NAS3-23901 and No. NCC3-221 is gratefully acknowledged. We also thank Prof. S. V. Patankar for providing to us an initial version of the gas-phase software.

References

Altenkirch, R. A., Eichhorn, R., and Shang, P. C., 1980, "Buoyancy Effects on Flame Spreading Down Thermally Thin Fuels," *Combust. Flame*, Vol. 37, pp. 71–83.

Altenkirch, R. A., Rezayat, M., Eichhorn, R., and Rizzo, F. J., 1982, "Boundary Integral Equation Method Calculations of Surface Regression Effects in Flame Spreading," ASME JOURNAL OF HEAT TRANSFER, Vol. 104, pp. 734–740.

Altenkirch, R. A., Eichhorn, R., and Rizvi, A. R., 1983, "Correlating Downward Flame Spread Rates for Thick Fuels," *Comb. Sci. Tech.*, Vol. 32, pp. 49–66.

Altenkirch, R. A., and Bhattacharjee, S., 1990, "Opposed-Flow Flame Spread With Implications for Combustion at Microgravity," *AIAA Prog. Aero. Astro.*, Vol. 130, pp. 723–740.

Bhattacharjee, S., and Altenkirch, R. A., 1990, "The Effect of Surface Radiation on Flame Spread in a Quiescent, Microgravity Environment," *Combust. Flame*, Vol. 84, pp. 160–169.

Bhattacharjee, S., Altenkirch, R. A., Srikantaiaih, N., and Vedha-Nayagam, M., 1990, "A Theoretical Description of Flame Spreading Over Solid Combustibles in a Quiescent Environment at Zero Gravity," *Comb. Sci. Tech.*, Vol. 69, pp. 1–15.

Bhattacharjee, S., and Altenkirch, R. A., 1991, "Radiation-Controlled, Opposed-Flow Flame Spread in a Microgravity Environment," *Twenty-Third Symposium (International) on Combustion*, The Combustion Institute, Pittsburgh, PA, pp. 1627–1633.

Bhattacharjee, S., Altenkirch, R. A., Olson, S., and Sotos, R. G., 1991, "Heat Transfer to a Thin Solid Combustible in Flame Spreading at Microgravity," ASME JOURNAL OF HEAT TRANSFER, Vol. 113, pp. 670–676.

de Ris, J. N., 1969, "Spread of a Laminar Diffusion Flame," *Twelfth Symposium (International) on Combustion*, The Combustion Institute, Pittsburgh, PA, pp. 241–252.

Di Blasi, C., Continillo, G., Crescitelli, S., and Russo, G., 1987, "Numerical Simulation of Opposed Flow Flame Spread Over a Thermally Thick Solid Fuel," *Combust. Sci. Tech.*, Vol. 54, pp. 25–36.

Di Blasi, C., Crescitelli, S., Russo, G., and Fernandez-Pello, A. C., 1988, "Prediction of the Dependence on the Opposed Flow Characteristics of the Flame Spread Rate Over Thick Solid Fuel," *Second International Symposium on Fire Safety Science*, Tokyo, Japan, June 13–17.

Fernandez-Pello, A. C., Ray, S. R., and Glassman, I., 1981, "Flame Spread in an Opposed Forced Flow: The Effect of Ambient Oxygen Concentration," *Eighteenth Symposium (International) on Combustion*, The Combustion Institute, Pittsburgh, PA, pp. 579–589.

Frey, A. E., and T'ien, J. S., 1979, "A Theory of Flame Spread Over a Solid Fuel Including Finite Rate Chemical Kinetics," *Combust. Flame*, Vol. 36, pp. 263–289.

Ito, A., and Kashiwagi, T., 1986, "Temperature Measurements in PMMA During Downward Flame Spread in Air Using Holographic Interferometry," *Twenty-First Symposium (International) on Combustion*, The Combustion Institute, Pittsburgh, PA, pp. 65–74.

Lengelle, G., 1970, "Thermal Degradation of Polymers," *AIAA Journal*, Vol. 8, pp. 1989–1996.

Mao, C. P., Kodoma, H., and Fernandez-Pello, A. C., 1984, "Convective Structure of a Diffusion Flame Over a Flat Combustible Surface," *Combust. Flame*, Vol. 57, pp. 209–236.

Olson, S. L., Ferkul, P. V., and T'ien, J. S., 1989, "Near Limit Flame Spread Over a Thin Solid Fuel in Microgravity," *Twenty-Second Symposium (International) on Combustion*, The Combustion Institute, Pittsburgh, PA, pp. 1213–1222.

Patankar, S. V., 1980, *Numerical Heat Transfer and Fluid Flow*, McGraw-Hill, New York.

Seshadri, K., and Williams, F. A., 1978, "Structure and Extinction of Counterflow Diffusion Flame Above Condensed Fuels: Comparison Between PMMA and Its Liquid Monomer, Both Burning in Nitrogen–Air Mixtures," *Journal of Polymer Science—Polymer Chemistry Edition*, Vol. 16, pp. 1755–1778.

Touloukian, Y. S., 1970, "Thermophysical Properties of Matter, The TPRC Data Series, IFI/Plenum.

West, J. S., Bhattacharjee, S., and Altenkirch, R. A., 1992, "A Comparison of the Roles Played by Natural and Forced Convection in Opposed-Flow Flame Spreading," *Combust. Sci. Tech.*, Vol. 83, pp. 233–244.